Jet Installation Noise Modelling Informed by GPU LES

Hussain A. Abid *, Annabel P. Markesteijn †, Vasily Gryazev ‡, and Sergey A. Karabasov §
School of Engineering and Material Science, Queen Mary University of London, Mile End Road, London

Hasan Kamliya Jawahar ¶ and Mahdi Azarpeyvand ‖
University of Bristol, Bristol, England BS8 1TR, United Kingdom

Jet installation beneath a wing significantly enhances jet noise at low frequencies, and its physical mechanism must be comprehended to develop efficient noise reduction solutions. A numerical investigation on the jet-installation noise is performed using Wall Modelled Large Eddy Simulation (WMLES) performed using the high-resolution CABARET method accelerated on Graphics Processing Units. To simulate jet installation, a flat plate is put outside of the jet's plume, causing a rise in noise levels due to the scattering of near-field hydrodynamic waves at the trailing edge of the plate. The configuration adopted in this work replicates a series of experiments performed at the University of Bristol, against which the numerical results are validated. The numerical simulation is performed for Mach numbers of 0.5 and 0.9, and the influence of the selected noise reduction technique, i.e., the usage of chevron nozzles in comparison with the baseline round nozzle, on the jet-installation is studied by modelling SMC006 chevron nozzle. The properties of jet-hydrodynamic pressure variations and their effect on nozzle type and Mach number are investigated. Far-field noise spectra from the isolated and installed jet cases, obtained through the Ffowcs-Williams Hawkings method, are compared at different polar angles. In addition, a hybrid semi-analytical hydrodynamic-edge scattering prediction model is implemented following the model of Lyu and Dowling [1] to analyse jet-installation noise, using inputs obtained directly from the LES calculation. The implemented model is found to capture the correct physics at peak jet installation frequencies and can be used as a robust prediction tool for jet-installation noise optimisation in the future.

I. Introduction

The advent of modern high-bypass area-ratio turbofan engines in modern commercial aircraft led to a significant benefit in engine-fuel efficiency and reduction of jet noise due to the decrease in the nozzle exhaust velocity. However, the increase in bypass ratio also increased the engine diameter. For typical jet-under-the wing configurations, this led to installing engines close to the wing to maintain the required ground clearance. Altogether this results in the increased interaction between the jet and the airframe, thereby leading to an increased low to mid-frequency noise referred to as the jet-installation (JI) effect. In a recent NASA study, Brown [2] showed that JI noise depends of the vertical position of the jet centre line with respect to the solid surface as well as the horizontal distance between the end of the jet potential core and the surface edge. It is also known that in some cases the jet flow-edge interaction effect may lead to acoustic tones [3]

In comparison with the pure jet mixing noise, which is largely related to turbulence-turbulence interactions, the mechanism of JI noise is associated with scattering of the hydrodynamic pressure field of the jet by the solid surface. The hydrodynamic pressure field is evanescent in isolated jets and it is the scattering effect of the solid surface which leads to its efficient propagation to the far field. The scattering effect is specially important at the trailing edge of the surface. Since the early works of [4–7] the dipole nature of the jet installation noise was recognised. In accordance with Curle's theory [8], the surface pressure fluctuations produced by the jet can be represented by distributing acoustic dipoles on the surface. Ffowcs Williams and Hall [9] developed an analytical model of sound scattering by the trailing edge of a semi-infinite flat plate assuming a quadrupole source close to the surface. An alternative sound scattering

*PhD. Student, School of Engineering and Materials Science
†Postdoctoral Research Assistant, School of Engineering and Materials Science / Director GPU-prime Ltd, Cambridge, UK
‡Postdoctoral Research Assistant, School of Engineering and Materials Science
§Professor of Computational Modelling, School of Engineering and Materials Science, AIAA Associate Fellow
¶Research Associate,Department of Aerospace Engineering
‖Professor in Aerodynamics and Aeroacoustics, Department of Aerospace Engineering

model was developed by Amiet [10], who considered pressure fluctuations induced on the surface close to the trailing edge as the effective acoustic source, which is scattered to the far field. In comparison with the Ffowcs Williams and Hall model, the Amiet trailing edge noise is simpler because it only requires a point source at the trailing edge for obtaining the far-field noise predictions and does not need a computation or measurement of the effective acoustic source in the volume. In particular, the Amiet model was used in the work of [11] who experimentally investigated the JI noise and developed a semi-analytical model for its prediction where the near-field hydrodynamic evanescent waves were used as the acoustic source and the scattering phenomenon was modelled based on Amiet's approach.

One of the ways to mitigate the jet-installation noise is to reduce the impact of the hydrodynamic waves impinging on the surface from jet, thereby reducing their scattering effect in the far field. Along this line of thought, application of chevron nozzles offers an opportunity to enhances the large-scale mixing, thereby breaking the large-scale coherent structures of the hydrodynamic field of the jet. For example, Bridges and Brown [12] analyzed the factors influencing the acoustic benefits of chevron nozzles and showed that the number of chevrons, the chevron length, and penetration angle strongly affect the peak jet noise associated with the large scale structures in the jet. More recently, Jawahar et al. [13] performed a series of experiments to investigate the effect of chevrons on jet-installation noise for a jet-flat plate configuration for several Mach numbers. Despite some interesting findings, for example, showing that the SMC006 chevron nozzle considered to be most efficient by Bridges and Brown [12] for isolated jets also leads to best reduction of the JI noise, the work also showed that the root mechanisms of JI noise are yet be understood. For further understanding, high-resolution space-time information of the jet flow and pressure fields is required, which may be challenging to obtain experimentally. At the same time, such high-resolution information can be provided from eddy-resolving modelling such as using Large Eddy Simulations (LES).

Hence, the goal of this paper is to perform a series of Wall Modeled LES (WMLES) calculations of the installed and isolated round and chevron jets from the experimental campaign of Jawahar et al. [13], validate the solutions in comparison with the experiment, and then analyse the LES flow fields in terms of the efficient sources of JI noise using the Amiet theory-based approach developed by Lyu et al. [11].

The WMLES calculations performed in this work are based on the high-resolution CABARET method [14–17] accelerated on Graphics Processing Units (GPU) [18]. The solver utilizes a GPU-optimized method for solving the hyperbolic part of the Navier-Stokes equations using the asynchronous time stepping at the optimal CFL number corresponding to a minimum dispersion and dissipation error [17, 19]. The CABARET method for jet flow and noise calculations was validated in [20–23] and for airfoil flows in [24, 25].

II. Numerical Setup

A. Installed jet configuration and flow condition

Installed jet configuration and flow condition are based on the experiments performed at the Bristol Jet Aeroacoustic Research Facility (B-JARF) at the University of Bristol, where the isolated jets are placed close to the flat plate [13].The test facility is well validated for a wide range of mach numbers[26–29]. The experiments were carried out for a round convergent nozzle (SMC 000) and four chevron nozzles. However, in this paper, we consider SMC006 chevron nozzle to investigate the influence of chevron on near-field properties of the jet and installed jet case. The tested nozzles are a 3:1 scaled-down version of the nozzle of the experiments by [2]. Hence the exit jet diameter used for the current analysis is $D_j = 16.933mm$. The flat plate has a length of $10D_j$ and a total span of $24D_j$ to avoid the scattering at the leading edge and spanwise side edges of the plate. The geometric configuration investigated in this simulation involves $L = 6.5D_j$, where L is the axial distance from the jet exit plane to the trailing edge of the plate. The surface is placed $H = 2D_j$ away from the surface to ensure that the jet plume doesn't graze the surface. Two exit Mach numbers are tested which are Mach = 0.5 and 0.9.

B. GPU Cabaret Method

Following the previous studies [23] , a suitable synthetic turbulence boundary condition is used upstream on the nozzle inlet in the GPU CABARET simulations, the size/thickness of the layer(s) near the boundary is controlled in the framework of the OpenFOAM snappyHexMesh routine, which involves adding body-fitted hexahedral layers near the viscous wall boundary. For example, during the automatic meshing procedure, the distance between the centre of the control volume closest to the boundary and the boundary itself can be kept within a certain distance. Following Park [30] the so-called equilibrium wall model is considered. The basic steps of the WMLES algorithm are implemented

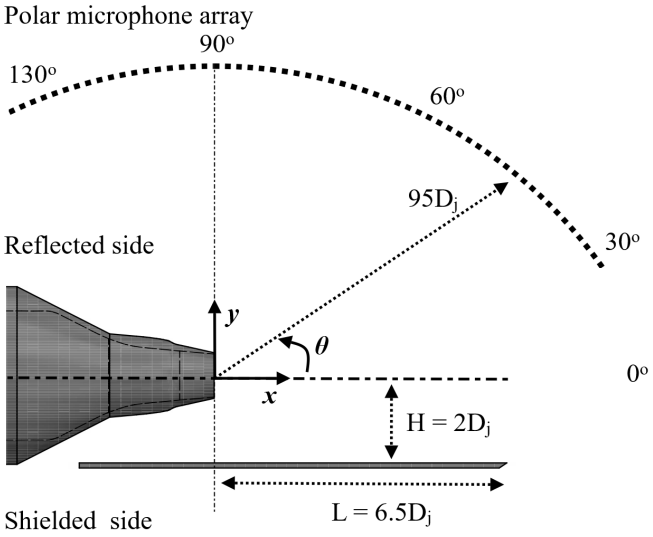

Fig. 1 Schematic of the jet-installation setup with $L = 6.5D_j$ and $H = 2D_j$

as follows. Inside the boundary layer mesh, each time step, the cell-centred values of the velocity (and density) are evaluated. These values are provided to the wall model, which, in turn, provide the wall shear stress. Consequently, this wall shear stress is used as a boundary condition for the LES at the wall. The wall model that has been employed here initially is based on the algebraic method using Reichardt's law as described in [31]. Reichardt's law of the wall gives a relation between the local u+ and the y+ of the wall, wherein the WMLES modelling assumed that the instantaneous velocity could be used as input to the wall law. The resulting non-linear algebraic equation for the velocity profile is solved by a simple Newton iteration, giving the wall shear stress.

Using the snappyHexMesh utility, the LES mesh has been generated from CAD geometry. Areas of the refined grid have been placed around the jet and the flat plate, which include the location of several acoustic integration surfaces in the framework of the [32] (FW-H) method, as shown in Fig. 3. Fig. 2 shows contours of vorticity magnitude (10000 1/s) and only the smallest (1st), 4th, and largest surface (8th) are shown for clarity. In all cases, 8-time update groups of the asynchronous time-stepping method have been used, corresponding to the factor of 2^7= 128 ratios between the time step used for the smallest and the largest grid cells. The simulations were run on Nvidia Volta V100 GPU cards. The round jet (SMC000-type) correspond to thinner initial shear layers in comparison with the chevron (SMC006-type) jets; thereby, finer grids were used in the former case. Moreover, the grid validation study was performed. The mesh and their corresponding grid sizes are are explained herein.

1. Isolated Jet

For the isolated round jet SMC000, two grid resolutions corresponding to 40 and 110.7 million cells are simulated. The grid at the nozzle lip-line for both meshes is close to Cartesian uniform with dx/D=dy/D=dz/D = 0.006. The FW-H surface has a conical shape with multiple closing discs. The maximum resolved Strouhal number near the nozzle corresponds to St=9 and St=4 near the end of the potential jet core, assuming the grid resolution of 8 points per acoustic wavelength (p.p.w.). The LES grids of 40 and 85 million cells were used for the isolated chevron SMC006 jet. In this case, the grid resolution at the nozzle lip corresponded to dx/D=dy/D=dz/D = 0.01. The maximum resolved Strouhal number near the nozzle corresponds to St=6 and St=3 near the end of the potential jet core, assuming the grid resolution of 8 p.p.w. The LES grid for isolated chevron jet is shown in Fig. 4.

2. Installed jet

Two grids were generated for the installed SMC000 jet case corresponding to 40 and 125.8 million grid points. The grid topology near the lip-line was similar to that of the isolated SMC000 nozzle. The installed chevron jet case SMC006 has a similar LES grid to the isolated SMC006 near the nozzle, and two corresponding grids simulated are comprised of 40 and 98 million cells. The near-field mesh, near the jet exit, and the lipline have a similar topology as the one shown in Fig. 4. The flat plate has a higher grid density from the nozzle exit to the trailing edge.

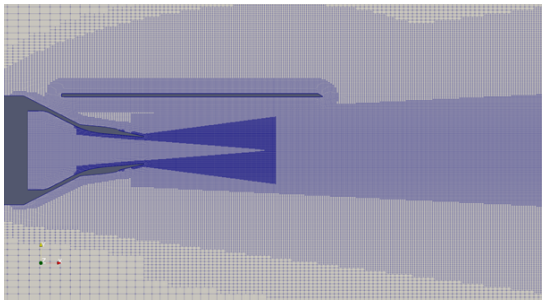

(a)

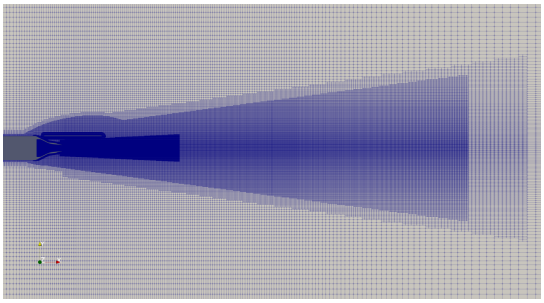

(b)

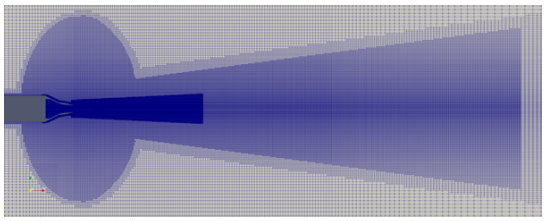

(c)

Fig. 2 LES grid for the installed jet configuration

Two FW-H formulations were performed for the installed jet case to calculate the far-field noise. The flow solver is coupled with the penetrable FW-H integral surface method in the first method. In this method, the flow solution is recorded on 16 integration surfaces, i.e. the closing discs, which confine the jet turbulence and vorticity region as shown in Fig. 3. Far-field sound is computed using the analytical free-field Green's function method. The second formulation involved the LES solution combined with the impenetrable FW-H surface, which coincided with the flat plate. The far-field noise spectra obtained using both methodologies are compared one with the other and with the experiment for all test cases under consideration.

3. Statistical Calculation and GPU Performance

The simulations were run for 300 convective time units (TUs; each TU is based on the nozzle exit diameter and jet velocity at the nozzle exit) for the initial-solution spinout and then a minimum of an additional 1100 TUs for statistical averaging. The GPU-LES calculations were performed on JADE-2 High-Performance Computing Facility comprising NVIDIA TESLA V-100 (32GB) GPU cards. The isolated jet simulations were performed on a single GPU configuration while the installed jet simulations were performed on 2GPUs to accelerate the computations.

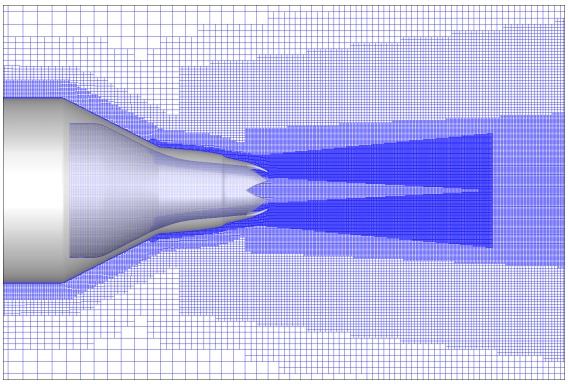

Fig. 4 LES grid in the vicinity of the Chevron SMC006 Nozzle

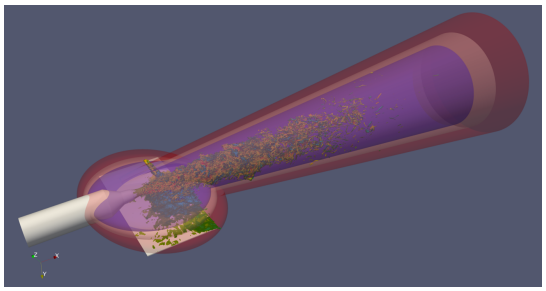

(a)

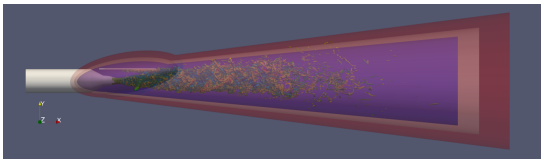

(b)

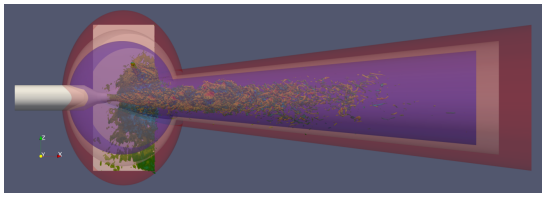

(c)

Fig. 3 Acoustic integration surfaces wrapped around the vorticity regions of the installed jet flow

Jet Installation Test Cases			
Case	Grid Size	GPUs	TUs/day
Isolated SMC000	40	1	380
Isolated SMC000	110.7	2	200
Isolated SMC006	40	1	480
Isolated SMC006	85	2	450
Installed SMC000	40	1	660
Installed SMC000	125.8	2	180
Installed SMC006	40	1	680
Installed SMC006	98	2	400

Table 1 Grid Characteristics and Solution turn-around time

C. Grid Sensitivity Study and Validation

The numerical grid sensitivity study is performed to assess the sensitivity of the numerical results to the discretization of the computational domain. For this purpose, we investigated two grid sizes for each of the test cases under consideration as described in Table 1. Each mesh has a similar mesh resolution near the nozzle exit and a variable resolution at downstream locations. The simulated results for isolated and installed SMC000 are compared with the experimental results for the time-averaged axial velocity profile and root-mean-square (RMS) axial velocity as shown in Fig. 5.

Fig. 5 shows the the comparison of the time-averaged normalized axial velocity profile with the experimental measurement of Brown [2]. The near-field was measured using particle Image Velocimetry (PIV) in the experiment at various streamwise and cross-stream locations. The near-field experimental data from Brown [2] is only available for an isolated test case. However, in the investigation of [13] and the current LES configuration, the plate is located at $H/D_j = 2.0$ and is far from the jet-potential core. Hence it is expected that there will be no difference in mean-velocity obtained from the isolated and the installed jets. Fig. 5 shows that the velocity profiles of the isolated jet at 40mln and 110.7mln are close to each other at streamwise locations, closer to the nozzle exit until $7D_j$. This shows that the grid density near the nozzle for 40mln cells is sufficient to resolve the flow statistics. For the installed jet case, the difference between 40mln and 125.8mln cells become slight significant by $7D_j$; but the profiles are closer together in the regions close to the nozzle exit.

Moreover, it can be observed that the results for installed jet mesh of 125.8mln cells match closely with the

experimental data, thereby signifying that the presence of the plate has negligible influence on the average jet properties and velocity profiles. Furthermore, the current results also show that the near-field hydrodynamic pressure is also unaffected by the existence of the plate, as we will see in Section IV.C.1

The current analysis demonstrates that a 40mln grid for an isolated and installed SMC000 jet gives acceptable accuracy in comparison to the experiments. Furthermore, comparable findings were observed for the SMC006 isolated and installed nozzles, which results were not included here for brevity. As a result, the existing numerical setup can be considered validated, Furthermore, for isolated/installed jet analysis of the SMC000 and SMC006 nozzles, the grid models of 40 million cells will be used.

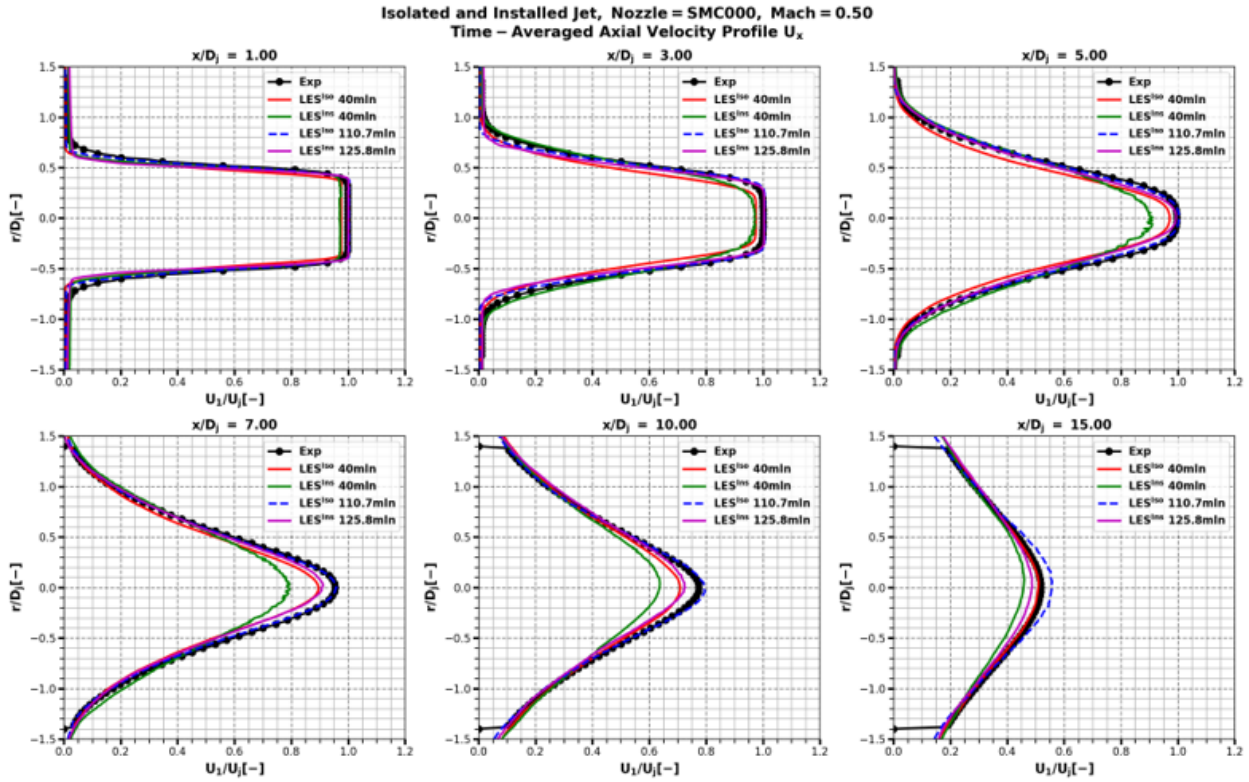

Fig. 5 Comparison of the the axial velocity profile at the various axial locations for the isolated and installed round jet SMC000 case at Mach = 0.5 for different grids with the PIV experimental measurement.

.

III. Acoustic noise models

In this section, the near-field hydrodynamic pressure - edge scattering model developed by Lyu and Dowling [1] for the modelling of the jet-installation noise is presented. The source parameters herein will be obtained from the LES simulation.

A. Hydrodynamic pressure trailing edge scattering model

Lyu and Dowling [33] developed a noise model for jet installation based on the similar analogy as the Amiet TEN model. The acoustic source of the Lyu and Dowling [33] model, unlike the Amiet model[10], is the azimuthal model of the near-field hydrodynamic pressure. The flat-plate is assumed to be outside the jet core so that the jet does not scratch the flat plate. As a result, the non-linear/linear part of the hydrodynamic field will be unaffected and hence can be used as a model source. The impingement of the hydrodynamic field on the airfoil surface is modelled as dipoles being distributed on the flat surface. The farfield acoustic pressure is then computed using the theories of Curle [8] and Kirchoff. The JI noise model is given by Eq. (1)

$$
\begin{aligned}
S_{pp}\left(x_1, x_2, x_3 = 0; \omega\right) = \frac{1}{\pi}\left[\frac{\omega x_2}{c_0 S_0^2}\right]^2 \sum_{m=0}^{N}\left|\frac{\Gamma\left(c,\, \mu|_{k_3 = k(x_2/S_0)}, \mu_A\right)}{\mu_A}\right|^2 \Pi_s(\omega, m) \\
\times\left\{\left(\sum_{k=0}^{|m|/2|} C_{|m|}^{2k} H^{-2k+1/2} \gamma_c^{-|m|} \frac{\mathrm{d}^{2k}}{\mathrm{d}k_3^{2k}}\left[\left(\gamma_c^2 + k_2^2\right)^{1/2|m|-1/4} K_{|m|-1/2}\left(H\sqrt{\gamma_c^2 + k_3^2}\right)\right]\right)^2\right. \\
\left.+\left(\sum_{k=0}^{||m|-1/2]} C_{|m|}^{2k+1} H^{-2k+1/2} \gamma_c^{-|m|} \frac{\mathrm{d}^{2k}}{\mathrm{d}k_3^{2k}}\left[k_3\left(\gamma_c^2 + k_3^2\right)^{1/2|m|-3/4} K_{|m|-3/2}\left(H\sqrt{\gamma_c^2 + k_3^2}\right)\right]\right)^2\right\}_{k_3 = k x_3/S_0}
\end{aligned} \tag{1}
$$

where c_o is speed of sound, U_c is the convection velocity of the turbulent eddies in the boundary layer, σ is flow corrected far-field observation location defined as $S_0^2 = x_1^2 + \beta_c^2\left(x_2^2 + x_3^2\right)$, $\beta_c = \sqrt{1 - M_\infty^2}$ is the compressibility correction. x_1 and x_2 are observer coordinates in streamwise and vertical direction. $\Pi_s(\omega, m)$ is the azimuthal modal spectra of near-field hydrodynamic pressure which is the source of the JI noise calculation. The near-field hydrodynamic pressure varies in axial and radial direction, hence for JI noise calculation, it is more reasonable to choose this point at the location where the trailing edge of the scattering surface is located. In this case, since the trailing edge is located at $H = 2D_j$ and $L = 6.5D_j$, the hydrodynamic pressure at this location will be obtained the LES simulation be used as an input to the JI noise model. Additionally, If we assume that the observer is located in the mid span i.e. $x_3 = 0$; and only mode 0 and mode 1 of hydrodynamic pressure field is important the model simplifies to Eq. (2).

$$
\begin{aligned}
S_{pp}\left(x_1, x_2, x_3 = 0; \omega\right) \approx \left[\frac{\omega x_2}{c_0 S_0^2}\right]^2 \left\{\left|\frac{\Gamma\left(c, \mu, \mu_A\right)}{\mu_A}\right|^2 \Pi_s(\omega, 0) \frac{\mathrm{e}^{-2H\gamma_c}}{2\gamma_c^2}\right\}_{k_3=0, m=0} \\
+\left\{\left|\frac{\Gamma\left(c, \mu, \mu_A\right)}{\mu_A}\right|^2 \Pi_s(\omega, 1) \frac{\mathrm{e}^{-2H\gamma_c}}{2\gamma_c^2}\right\}_{k_3=0, m=1}
\end{aligned} \tag{2}
$$

Lyu and Dowling [33] assumed that only mode 0 and 1 were significant for JI noise hence the model can be simplified version of the model is shown in Eq. (2); however, in this paper, we will be investigating the sensitivity of the model to number of azimuthal modes for SMC000 and SMC006. The computation of jet-installation noise using Lyu and Dowling [33] informed by the spectra obtained from LES is shown in Section IV.C.

IV. Results and Discussion

A. Near-field flow statistics

The radial profiles of near field axial mean and fluctuating flow of the flow for installed and isolated round SMC000 jet is shown in Figs. 6 and 7. The LES prediction for the installed and isolated jet matches with each other for all axial locations, with small differences observed at the centerline at downstream locations of x/D_j. This shows that the existence of the plate at $2D_j$ vertically above the jet centerline has negligible effects on the mean and fluctuating axial velocity profiles. Similar results is observed for the SMC006 nozzle installed underneath the plate and have not been shown for brevity. Hence the outcome of the following profile is that the existence of the plate has a negligible effect on the near-field mean profiles; this means that the plume of the jet doesn't graze the lower surface of the plate; Hence the noise heard in the far-field is solely due to jet noise and edge scattering at the trailing edge.

B. Farfield noise results

This section compares the far-field noise spectra obtained using the LES simulation in conjunction with the FW-H technique for isolated and installed jet case for all three nozzles at Mach number of 0.5 and 0.9.

1. Isolated Jet Noise

The permeable FW-H formulation with 16 closing discs is used to predict the farfield noise spectra for isolated jets at both Mach values. The noise spectra at 30°, 60°, 90° and 110° are shown in Fig. 8. As the Mach number increases

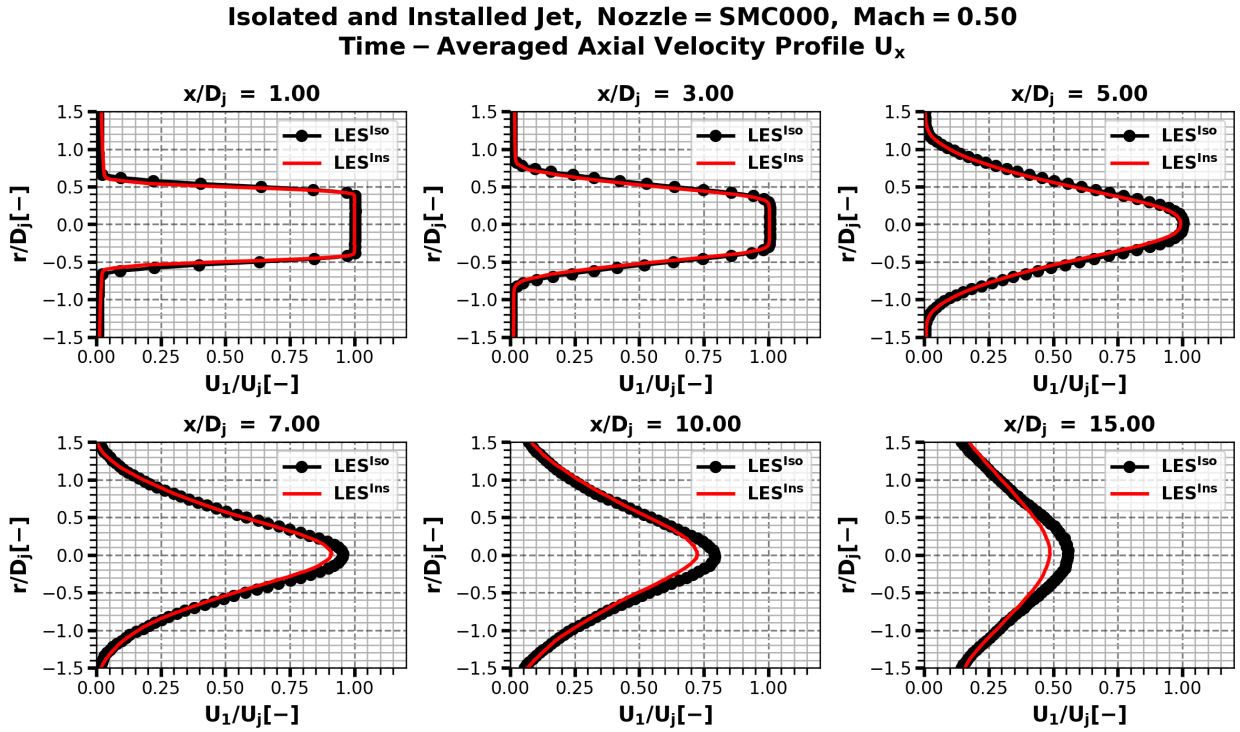

Fig. 6 Radial profile of time-averaged axial velocity at axial location of x/D_j = 1,2,5,7,10 and 15 for isolated round jet SMC000 nozzle at Mach = 0.5. black solid line: profile for isolated jet; red dashed line: profile for installed jet

.

from 0.5 to 0.9, the noise level rises as expected since the jet noise scales with the power of 8 with the jet Mach number. Furthermore, the LES-FWH formulation has been able to accurately forecast the noise at all polar angles for all of the nozzles at both Mach numbers, as can be seen from Fig. 8. This demonstrates that the existing grid of 40 million cells, together with the FW-H configuration, is adequate for accurate jet-noise computation. Further, as the Mach number increases, the characteristic frequency (frequency at which the peak spectral amplitude occurs) shifts to a higher-frequency regime (i.e. 2000Hz to above 4000Hz for Mach = 0.9), and this trend is visible for both nozzles. This is to be expected, as the production of tiny scale eddies is aided by greater Mach numbers, resulting in quadruple interaction and increased noise.

The effect of the nozzle shape on the noise radiated can also be visualised from Fig. 8. In comparison to the noise emitted by the SMC000 jet for Mach = 0.5, the noise emitted by SMC006 is decreased. Similar trend is observed for Mach = 0.9. However, overall sound pressure level (OASPL) at variable polar angle should be computed for better comparison.

2. Installed Jet Noise

This section compares the far-field noise spectra of the installed jet case with the experimental measurement for SMC000 and SMC006 for Mach number of 0.5 and 0.9. Fig. 9 shows the power spectral density (PSD) of the acoustic pressure for SMC000 and SMC006 installed underneath a flat plate, with the surface being $H = 2.0D_j$ in the radial direction and the trailing edge being at $L = 6.5D_j$. The observer is located on both the reflected and shielded sides of the surface.

The most dominant feature in Fig. 9 is the amplitude amplification at low frequency, an evident characteristic of the jet-installation noise. Comparing this with Fig. 8 signifies that scattering the pressure at the edge of the surface is the phenomenon of noise enhancement at low frequency. This agrees with the already established observation on jet installation. For both nozzles installed underneath the surface, the most considerable amplification is observed at frequency of 800 to 1000 Hz which is equal to a St of 0.1, with the difference of about 12-14dB with the spectrum of the

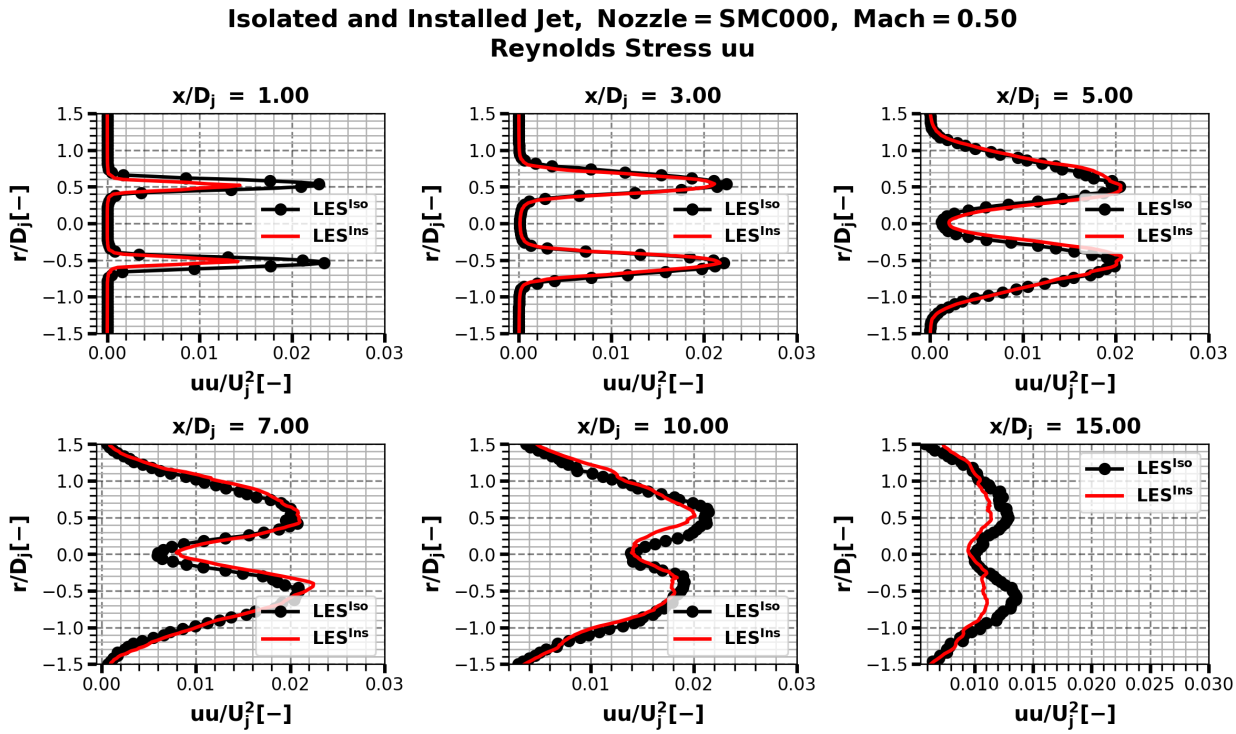

Fig. 7 Radial profile of root-mean-square axial velocity fluctuation at axial location of x/D_j = 1,2,5,7,10 and 15 for isolated round jet SMC000 nozzle at Mach = 0.5. black solid line: profile for isolated jet; red dashed line: profile for installed jet

.

isolated jet at same frequency range. Moreover, the spectra on shielded and reflected sides at low frequency are similar, consistent with the observations of [4]. This observation implies that the noise source is located at the trailing edge, such that there is negligible influence of sound reflection or shielding by the surface, and the total contribution to low frequency is due to the scattering phenomenon. [1, 11, 33] experimentally investigated the scattering phenomenon and showed that if the jet plume is away from the surface, the near-field hydrodynamic pressure field is scattered by the trailing edge to the far-field. Hence the noise mechanism for low-frequency regions is the near-field hydrodynamic pressure field. Lyu et al. [11] has also developed an analytical low-order model, the source parameter of which is obtained the LES. For the Strouhal number St>0.5, the spectra of the installed case are dominated by the jet noise or quadrupole noise. Beyond St>0.5, it can be seen that there is a 2-3dB difference between the reflected spectrum or isolated jet spectrum or shielded spectrum. This spectral increase at high frequency is associated with the reflection of the jet acoustic wave by the surface to the far-field.

Fig. 9 also shows the jet-installation effects at various observer angles. It is observed that the peak noise occurs at (800-1000Hz) corresponding to 0.1 Strouhal number, and the peak spectral level increases with increasing observer angle. The jet installation effects are maximum at a 90° observer angle on the reflected side of the plate. Additionally, the comparison of noise prediction using two different LES and FW-H methodologies is shown. In the first methodology, pressure signal is obtained using several acoustic integration surfaces (16 closing discs in this case) to compute the far field noise. The second method is the impenetrable FW-H in which the the unsteady surface pressure on the flat-plate is stored and Curle's methodology is employed to obtain the far-field acoustic pressure. For Mach = 0.5, it is observed that both of the formulations at all polar angles are able to predict the far-field noise accurately, including the peak at 30°, characteristic location for peak isolated jet noise. However, for Mach = 0.9, the employed impenetrable FW-H results in underestimation of the noise prediction at 30° while showing the accurate prediction at all polar angles. This is associated with the fact that impenetrable formulation, mostly computes the dipole-type noise (which is mostly enhanced at low Mach number), while cannot predict the quadruple noise, which is enhanced at increased Mach number. Similarly, the installed jet noise is slightly reduced for SMC006 in comparison with SMC000.

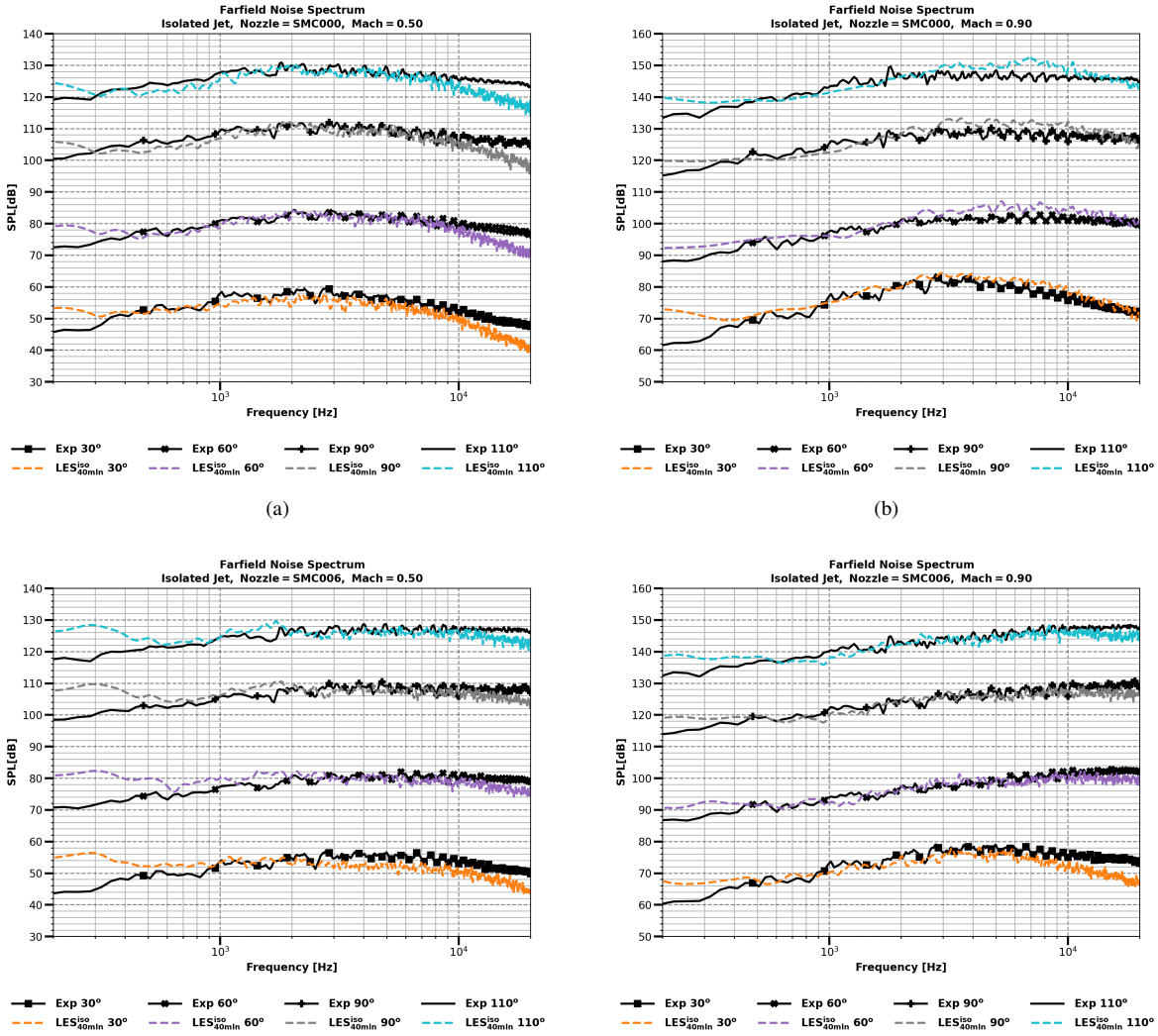

Fig. 8 Comparison of the farfield noise for Isolated SMC000 and SMC006 nozzle with the experimental measurement at Mach = 0.5 and 0.9 at polar angles of 30°, 60°, 90° and 110°. Note that 30° is the baseline, and the spectrum at remaining locations are shifted by 30dB for clarity

Overall, using the flat-plate as the FW-H surface provides for accurate prediction of peak far-field noise at almost all observer angles for all Mach numbers and nozzles. However, there is a 1-2dB difference in the measurement of 270-degree observer angles (shielded side). The noise is accurately captured at other observer angles. This means that at these observer angles, edge-scattering events dominate the installation effect. This is a significant finding since it enables the use of the SP spectrum at the trailing edge for noise prediction using the Amiet Model [10] or develop noise jet installation noise modelling techniques employing the statistics on the plate surface. As a result, any low-order modelling based on the Amiet model technique will require accurate SP spectrum calculation to predict jet-installation effects. The implication of this observation is tested in Section IV.C.

C. Jet Installation noise source and trailing edge scattering

The acoustic source for the jet-installation noise is the near-field hydrodynamic pressure fluctuation. The instantaneous pressure field for the isolated and installed jet case is shown in Fig. 10 to visualize the pressure waves emanating from the jet. The instantaneous pressure field indicates that the quadrupole source generates the jet noise. In

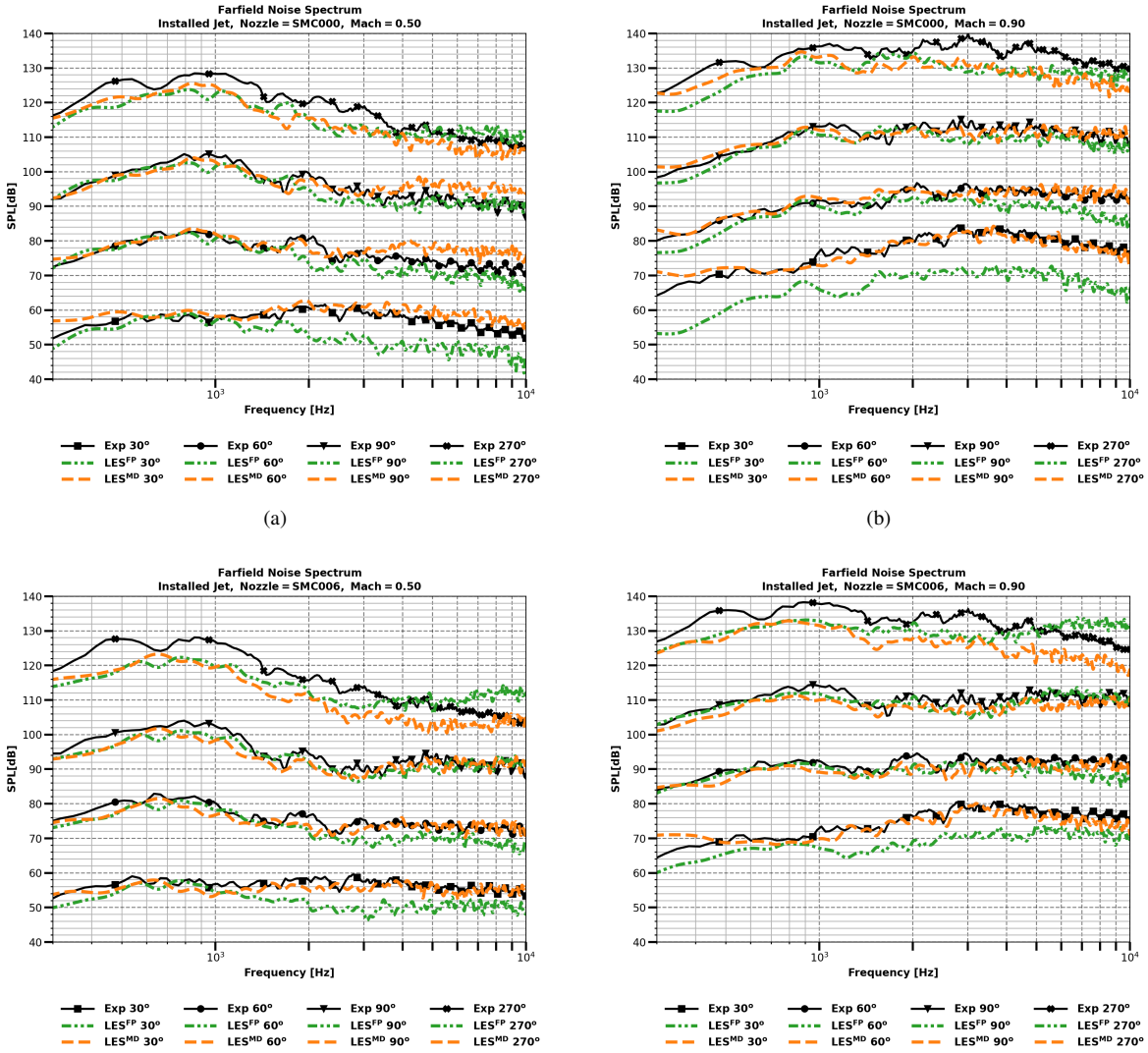

Fig. 9 Comparison of the far-field noise for Installed SMC000 and SMC006 nozzle using permeable and impenetrable FWH formulation with the experimental measurement at Mach = 0.5 and 0.9 at polar angles of 30°, 60°, 90° and 270°. Note that 30° is the baseline, and the spectrum at remaining locations are shifted by 20dB for clarity; Superscript FP represents employing flat-plate as FWH surface and MD represented employing LES and multiple closing discs.

contrast, Fig. 10b shows that the pressure field interaction with the plate modifies the field such that dipole pressure dilation is observed. The additional pressure region at the trailing edge is a consequence of the jet-pressure field interacting with the sharp edge. The sharp edge acts as a surface discontinuity and the jet-pressure field, which impinges on the surface, undergoes a resistance from unbounded to bounded region, i.e. surface. This phenomenon leads to non-propagating hydrodynamic pressure propagating acoustic pressure, which is heard as a low-frequency noise in the far-field acoustic spectrum as shown in Fig. 9. Fig. 10 also shows the cardioid directivity of the pressure wave, which is known to be distinctive of half-plane edge scattering. To further investigate the noise prediction using JI noise model, the source (i.e. near-field hydrodynamic pressure) is validated against the experimental results in Section IV.C.1 and then input into the Eq. (1) for JI noise prediction.

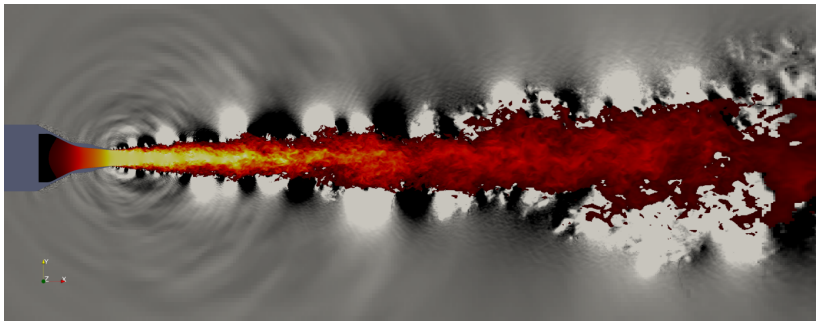

(a)

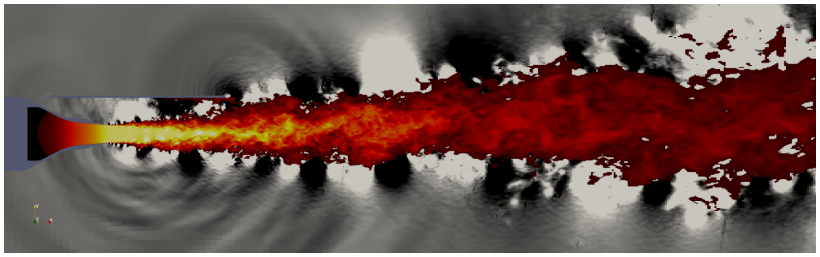

(b)

Fig. 10 Instantaneous pressure field (a) Isolated SMC000 (b) Installed SMC000

1. Near-Field Hydrodynamic Pressure

Fig. 11 shows the comparison between the experimental measurement [29] and the LES calculation to validate the near-field hydrodynamic pressure field for isolated SMC000 and SMC006 at Mach number of 0.5 and 0.9. The hydrodynamic pressure spectra are plotted at two locations corresponding to $x/D_j = 6.0, y/D_j = 2.0$ and $x/D_j = 14.0, y/D_j = 3.0$. The locations are chosen at end of the jet potential core,i.e. $x/D_j = 6.0$ and far downstream $x/D_j = 14.0$ and radial locations located outside jet-shear layer. From Fig. 11, we observe excellent agreement between the LES prediction and experiment for both nozzles at all location for both of the Mach numbers.This shows that the mesh is suitable enough to predict the near-field pressure field atleast upto $x/D_j = 14.0$ and that the LES solution can be considered validate and can be employed as the input to the JI noise model.

Fig. 11 also shows the characteristic features of the near-field hydrodynamic pressure domain. For instance, the hump at low frequency is observed, which shifts towards lower frequency with the increase of the Mach number, and axial location. This is because, with increased axial location in the flow domain, the flow evolves and the hydrodynamic pressure in the downstream location are mainly caused by the large scale eddies, hence hump is observed at lower frequency. Moreover, in Fig. 11, we have showed the comparison of hydrodynamic field by isolated jet with the experimental measurement by the isolated jet. Since, in current jet-installation case, no grazing of the jet potential core with the plate occurs as the plate is located at $L = 6.5D_j$ and$H = 2D_j$, it is expected that the hydrodynamic-pressure field will be unmodified by the existence of the plate. This is further investigated by comparing the near-field pressure obtained from isolated and installed jet case at two axial location $x/D_j = 2.0, y/D_j = 2.0$ (before the end of jet-potential core) and $x/D_j = 6.0, y/D_j = 2.0$ (end of jet potential core and point closest to the trailing edge). The comparison is shown in Fig. 12 and it is evident that the existence of the plate in current configuration doesn't influence the near-field pressure. Hence for JI noise prediction, the hydrodynamic pressure obtained from the isolated jet can be employed as a source for the noise prediction. for the JI noise prediction, the point in space is chosen to be $x/D_j = 6.5, y/D_j = 2.0$ as this corresponds to the location, where the trailing edge is located and where the hydrodynamic pressure will be scattered into acoustic waves resulting in enhanced farfield noise.

2. Surface Pressure Fluctuation

Fig. 13 shows the surface pressure (SP) spectrum on the flat plate at various spanwise and chordwise locations on the reflected side of the flat plate. The first distinctive feature is that the peak spectral level is observed at Stouhal number = 0.1. This peak spectral level translates to peak far-field spectral level, as shown in Fig. 9a. This clearly

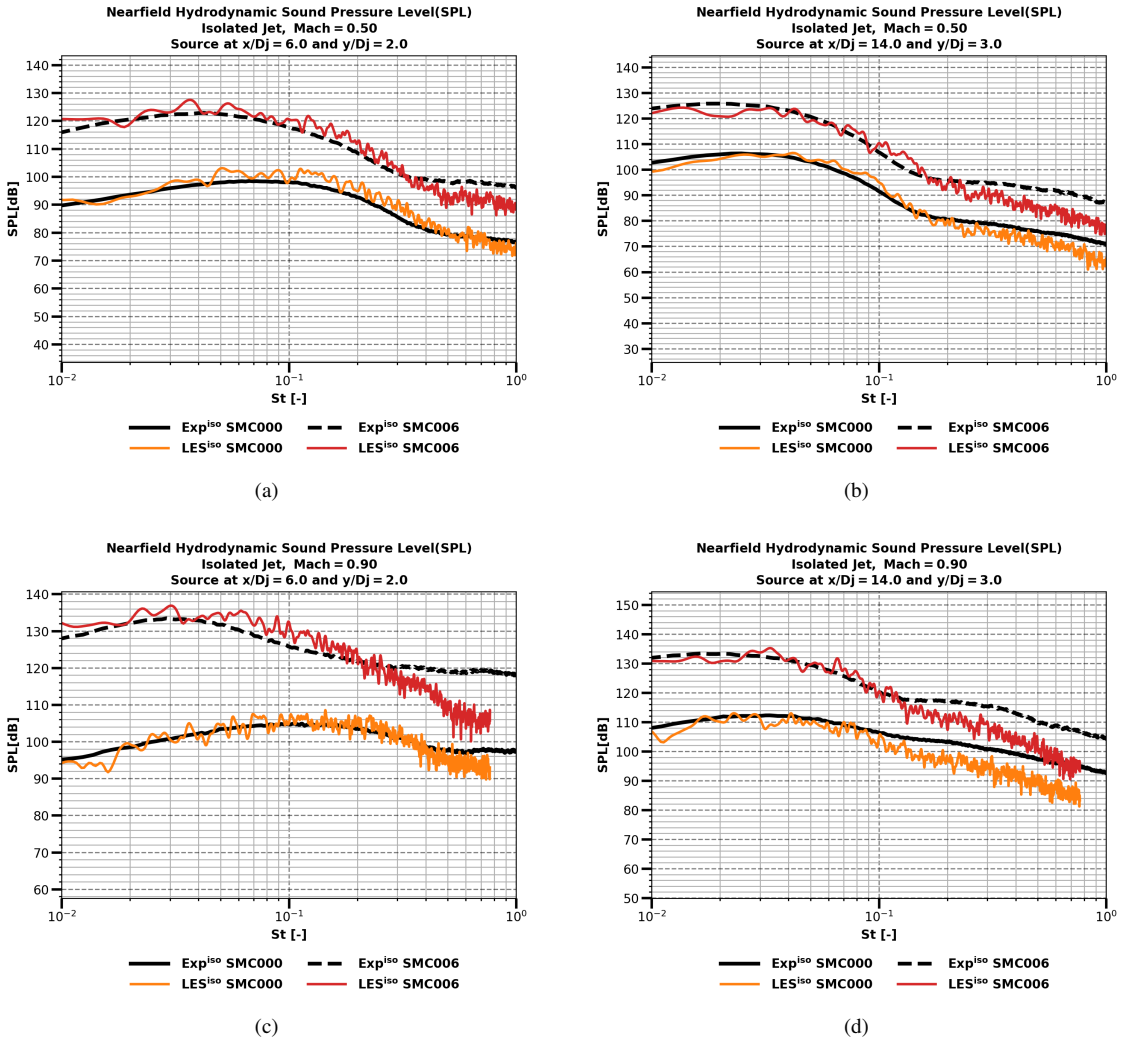

Fig. 11 Comparison of the predicted near-field hydrodynamic pressure with experimental measurement for isolated SMC000 and SMC006 at Mach = 0.5 and 0.9. (a) Mach = 0.5: $x/D_j = 6.0, y/D_j = 2.0$ (b) Mach = 0.5: $x/D_j = 14.0, y/D_j = 3.0$ (c) Mach = 0.9: $x/D_j = 6.0, y/D_j = 2.0$ (d) Mach = 0.9: $x/D_j = 14.0, y/D_j = 3.0$. Note that spectra are shifted 20dB for clarity

identifies that surface pressure spectrum on the surface of the flat-plate translates into farfield noise implying that, for any low-order modelling approach, such as those based on Amiet [10], can employ SP spectrum as a source. Moreover, the influence of the jet spreading in the spanwise direction can also be visualised in Fig. 13a. It is observed that SP spectral level is maximum at the mid plane of the flat plate, which coincides with the jet-center-line.The influence of the jet depletes in the spanwise location for a fixed chord length. For SMC000, the influence of the jet on the SP spectrum reduces and become insignificant by $5D_j$. Similar trend is observed for SMC006 chevron nozzle as well. The surface pressure (SP) spectrum obtained from the LES can be employed as an input to the Amiet [10] model. However, this is outside the scope of this paper, and further research on the viability of using SP spectrum as a source for modelling JI noise is recommended.

3. Jet Installation Noise Modelling

We compute the jet-installation noise in this part using the JI noise model given by Eq. (1). The azimuthal mode of the near-field hydrodynamic pressure is the source of the JI noise model. To get the azimuthal modal spectra, 64 points in

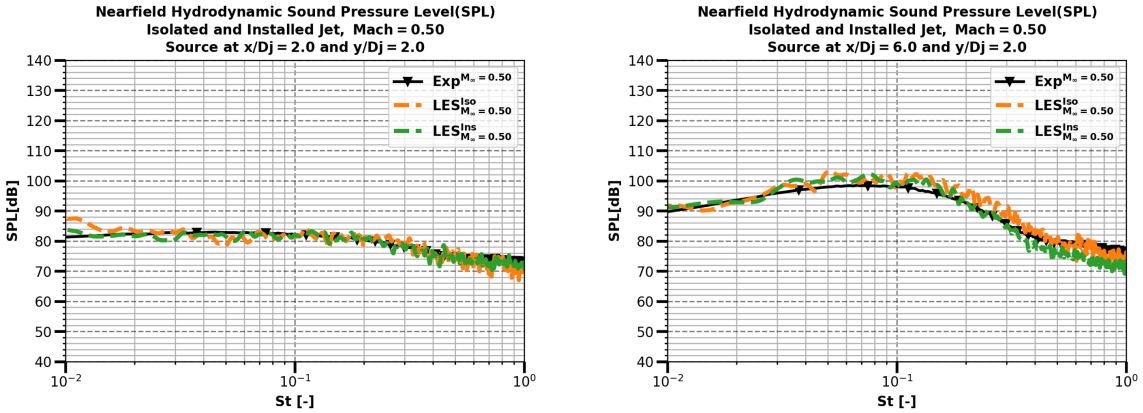

(a) (b)

Fig. 12 Comparison of the predicted near-field hydrodynamic pressure with experimental measurement for isolated and installed SMC000 at Mach = 0.5. (a) Mach = 0.5: $x/D_j = 2.0, y/D_j = 2.0$ (b) Mach = 0.5: $x/D_j = 6.0, y/D_j = 2.0$

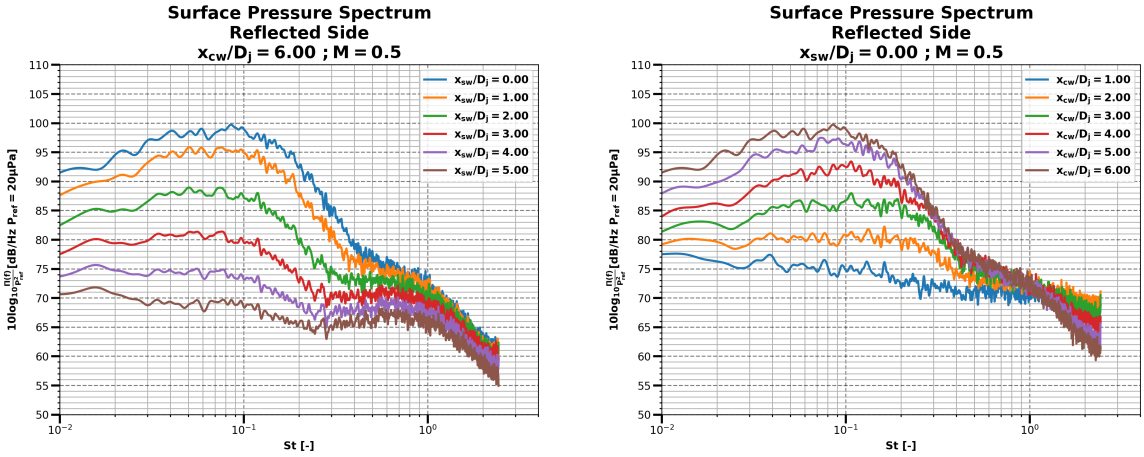

(a) (b)

Fig. 13 Surface Pressure Spectrum for Installed SMC000 at Mach = 0.5(a) fixed chordwise location and variable spanwise location (b) Variable chord-wise positions at the flat-plate mid-plane

the azimuthal direction were stored for each test case, and the fourier transform in the azimuthal direction was performed. Six azimuthal modes were calculated for the noise computation. Another input to the Eq. (1) is frequency-dependent convection velocity of the near-field instability waves. The convection velocity was determined using the methodology suggested in Lyu et al. [11] and it was observed that the convection velocity scaling for low frequency below Strouhal number of 0.15 did not differ for each mode, so the convection velocity was chosen to be constant for all modes in the current analysis. After computing the convection velocity, the azimuthal mode of the near-field pressure was obtained and input into the model at $x/D_j = 6.5, y/D_j = 2.0$. This was chosen as the source point since the trailing edge of the flat plate was located at this location, and the hydrodynamic pressure at this point will act as an incidence pressure to be scattered by the edge in the acoustic wave.

Fig. 14 shows the the prediction of the JI noise using the Lyu et al. Lyu et al. [11] hydrodynamic edge scattering model with the input of the source obtained from the LES. The JI noise is modelled for round (SMC000) and chevron (SMC006) nozzle for Mach = 0.5 and 0.9. The first observation is that the model has been able to predict the low-frequency noise with appreciable accuracy for all Mach number and nozzles. for example, Fig. 14a shows the peak frequency occurring

at a frequency of 1000Hz for Mach = 0.5 and 2000 Hz for Mach 0.9 for SMC000. The trend of the low frequency has been appreciably predicted. The discrepancies are observed at higher frequencies. This is due to the incorporation of the Amiet [10] transfer function, which is known the decay the high-frequency with a faster rate. Moreover, high frequency region of higher mode (mode > 1) decay faster, hence incorporation of higher modes yields discrepancies at higher frequency. Moreover, another explanation for the high-frequency difference is that the contributions from the quadrupole source, which normally influences the high-frequency region of the spectrum, were not taken into account in the prediction.

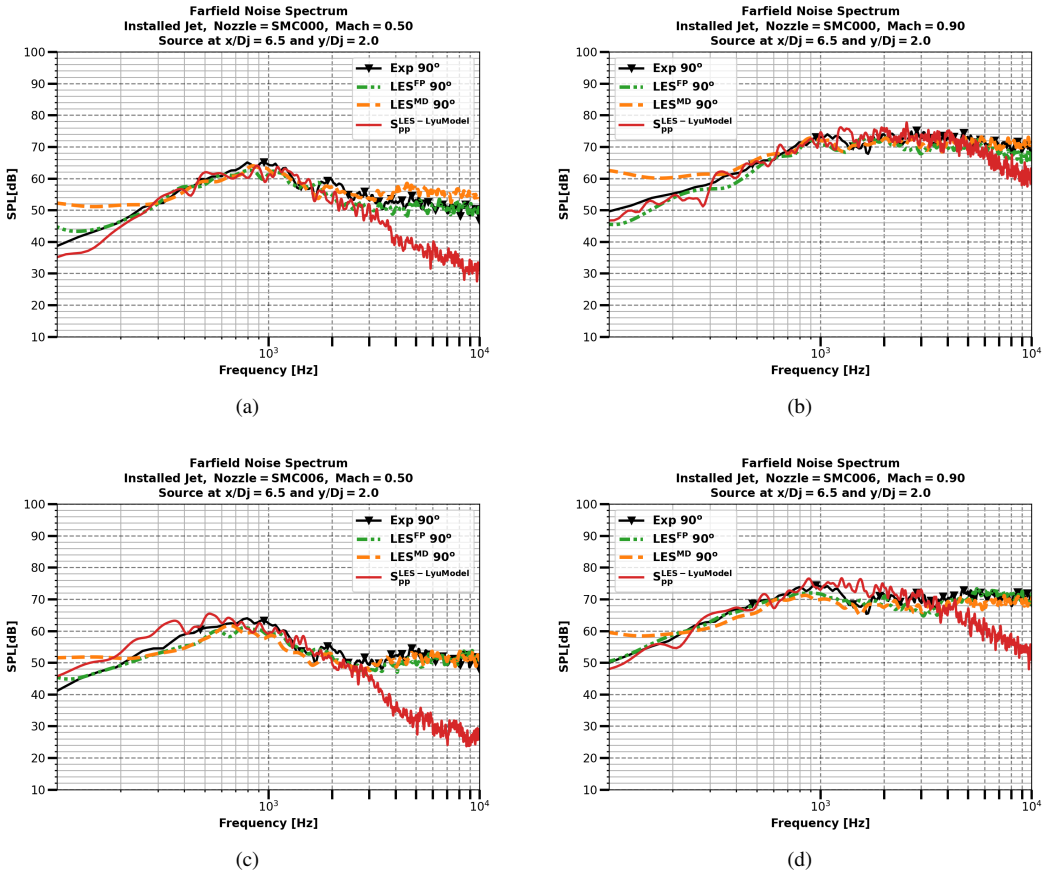

Fig. 14 Comparison of the model predicted farfield noise for Installed SMC000 and SMC006 nozzle with the experimental measurement and LES and FWH formulation at Mach = 0.5 and 0.9 at polar angles of 90°. Hydrodynamic pressure is obtained at $x/D_j = 6.5, y/D_j = 2.0$ (a) SMC000, Mach = 0.5 (b) SMC000, Mach = 0.9 (c) SMC006, Mach = 0.5 (d) SMC006, Mach = 0.9

Lyu et al. [11] model provided in Fig. 14 shows that the farfield acoustic pressure spectrum can be computed by performing the summation over the azimuthal modal spectrum. However, Lyu and Dowling [1] showed that when the frequency of interest is low, the farfield noise due to hydrodynamic pressure scattering can be obtained by using the power spectral density at a fixed point. This observation was shown to be valid for round jet at Mach = 0.5. However, no such information is available for the modelling of JI noise due to the chevron jet and at Mach number closer to sonic speeds. We investigate the sensitivity of the number of azimuthal mode required for noise modelling. The noise prediction for the installed SMC006 nozzle at Mach 0.5 and 0.9 is shown Figs. 14c and 14d.The prediction of the spectrum at Mach 0.5 required the inclusion of the first three azimuthal modes, and at Mach 0.9, the first four modes were necessary. The 0th mode is sufficient for SMC000 at Mach 0.5, however the first two modes are necessary for accurate predictions at Mach = 0.9.

Overall, the azimuthal modes of the hydrodynamic pressure as obtained from the LES simulation have been sufficient in predicting the noise caused by installed round and chevron jet.

V. Conclusion

A numerical investigation based on Large Eddy Simulation (LES) solutions provided by the high-resolution CABARET method accelerated on Graphics Processing Units is carried out to analyse the jet installation effects, together with the effects of varying jet Mach number and nozzle shape on the installed jet noise. For this purpose, a simplified configuration, comprised of round and chevron nozzle installed underneath the flat plate is chosen based on experimental tests performed at the University of Bristol. The simulation results are firstly validated by comparing the time-averaged velocity profile at various radial locations with the experimental data. The far-field noise spectra of isolated and installed jets are obtained using the Ffowcs Williams- Hawkings (FW-H) method, and it is found that the existence of the plate causes the jet noise to be enhanced significantly at low frequencies. For the isolated jets, the far-field noise is computed using the permeable-surface FW-H formulation with multiple closing surfaces. For the installed jets, the far-field noise is computed using two formulations of the FW-H method. In the first formulation, the permeable-surface FW-H method with multiple permeable closing discs is chosen, in the second method, the LES solution is combined with the impenetrable surface formulation of the FW-H method by employing a flat plate as the control acoustic surface. Notably, good agreement is observed using both methods at a range of observer angles except for a polar angle of 30 degrees, where the prediction using the impenetrable surface formulation results in underestimated noise in comparison with the permeable surface FW-H method and the experiment. Furthermore, the LES solution of the source of the jet-installation noise, i.e., the jet nearfield hydrodynamic pressure is validated with the experimental measurements. It is also shown that the presence of the plate for the current jet-flat plate setup does not modify the near-field pressure appreciably. To further analyse the origins of the jet-installation noise source in the considered experiments, the LES solution is substituted in the hydrodynamic pressure - edge scattering model of Lyu and Dowling [1]. It is shown that the implemented model leads to good agreement with the experiment for the low-frequency noise enhancement caused by instability wave scattering for all Mach numbers and nozzle shapes considered. This agreement demonstrates that the implemented near-field scattering model accurately captures the noise process for low-frequency noise amplification and provides a robust and reliable prediction tool for modelling jet installation effects. Notably, while it is sufficient to include just the axisymmetric mode for good predictions of jet installation noise of round jets, which is in-line with conclusions of the work of Lyu and Dowling [1], the minimum number of azimuthal modes required for accurate noise predictions of chevron nozzles should be significantly increased.

Acknowledgments

The authors would like to acknowledge the Engineering and Physical Sciences Research Council (EPSRC) for supporting this research (Grant No. EP/S000917/1 and EP/S002065/1). Sergey A. Karabasov gratefully acknowledges the financial support provided by the Ministry of Science and Higher Education of the Russian Federation (Grant agreement of December 8, 2020 № 075-11-2020-023) within the program for the creation and development of the World-Class Research Center "Supersonic" for 2020-2025. The authors also acknowledge the use of Tier-2 high-performance computing (HPC) facility JADE-2, funded by the EPSRC on the grant (EP/T022205/1) and Queen Mary's Apocrita HPC facility, supported by QMUL Research-IT. http://doi.org/10.5281/zenodo.438045

References

[1] Lyu, B., and Dowling, A. P., "Experimental validation of the hybrid scattering model of installed jet noise," *Physics of Fluids*, Vol. 30, No. 8, 2018, p. 085102. https://doi.org/10.1063/1.5036951, URL https://doi.org/10.1063/1.5036951.

[2] Brown, C. A., "Jet-Surface Interaction Test: Far-Field Noise Results," *Journal of Engineering for Gas Turbines and Power*, Vol. 135, No. 7, 2013, p. 071201. https://doi.org/10.1115/1.4023605.

[3] Jordan, P., Jaunet, V., Towne, A., Cavalieri, A. V. G., Colonius, T., Schmidt, O., and Agarwal, A., "Jet–flap interaction tones," *Journal of Fluid Mechanics*, Vol. 853, 2018, p. 333–358. https://doi.org/10.1017/jfm.2018.566.

[4] Head R., F. M., *Jet/surface interaction noise - Analysis of farfield low frequency augmentations of jet noise due to the presence of a solid shield*, ???? https://doi.org/10.2514/6.1976-502, URL https://arc.aiaa.org/doi/abs/10.2514/6.1976-502.

[5] Way, D., and Turner, B., "Model tests demonstrating under-wing installation effects on engine exhaust noise," *6th Aeroacoustics Conference*, 1980. https://doi.org/10.2514/6.1980-1048.

[6] Shearin, J. G., "Investigation of jet-intallation noise sources under static conditions," *Technical Report 2181, NASA Technical paper.*, 1983.

[7] Mead, C., and Strange, P., "Under-wing installation effects on jet noise at sideline," *4th AIAA/CEAS Aeroacoustics Conference*, 1998. https://doi.org/10.2514/6.1998-2207.

[8] N., C., "The influence of solid boundaries upon aerodynamic sound," *Proc. R. Soc. A*, Vol. 231, 1955, p. 505.

[9] Williams, J. E., and Hall, L. H., "Aerodynamic sound generation by turbulent flow in the vicinity of a scattering half plane," *Journal of Fluid Mechanics*, Vol. 40, No. 4, 1970, pp. 657–670. https://doi.org/10.1017/S0022112070000368.

[10] Amiet, R., "Noise due to turbulent flow past a trailing edge," *Journal of Sound and Vibration*, Vol. 47, No. 3, 1976, pp. 387–393. https://doi.org/https://doi.org/10.1016/0022-460X(76)90948-2.

[11] Lyu, B., Dowling, A. P., and Naqavi, I., "Prediction of installed jet noise," *Journal of Fluid Mechanics*, Vol. 811, 2017, p. 234–268. https://doi.org/10.1017/jfm.2016.747.

[12] Bridges, J., and Brown, C., *Parametric Testing of Chevrons on Single Flow Hot Jets*, ???? https://doi.org/10.2514/6.2004-2824, URL https://arc.aiaa.org/doi/abs/10.2514/6.2004-2824.

[13] Jawahar, H. K., Markesteijn, A. P., Karabasov, S. A., and Azarpeyvand, M., *Effects of Chevrons on Jet-installation Noise*, ???? https://doi.org/10.2514/6.2021-2184, URL https://arc.aiaa.org/doi/abs/10.2514/6.2021-2184.

[14] Karabasov, S., and Goloviznin, V., "Compact Accurately Boundary-Adjusting high-REsolution Technique for fluid dynamics," *Journal of Computational Physics*, Vol. 228, 2009, pp. 7426–7451. https://doi.org/10.1016/j.jcp.2009.06.037.

[15] Tucker, P. G., and Karabasov, S. A., "Unstructured Grid Solution of the Eikonal Equation for Acoustics," *International Journal of Aeroacoustics*, Vol. 8, No. 6, 2009, pp. 535–553. https://doi.org/10.1260/147547209789141498, URL https://doi.org/10.1260/147547209789141498.

[16] Chintagunta, A., Naghibi, S., and Karabasov, S., "Flux-corrected dispersion-improved CABARET schemes for linear and nonlinear wave propagation problems," *Computers Fluids*, Vol. 169, 2018, pp. 111–128. https://doi.org/https://doi.org/10.1016/j.compfluid.2017.08.018, recent progress in nonlinear numerical methods for time-dependent flow transport problems.

[17] Semiletov, V., and Karabasov, S., "CABARET scheme with conservation-flux asynchronous time-stepping for nonlinear aeroacoustics problems," *Journal of Computational Physics*, Vol. 253, 2013, pp. 157–165. https://doi.org/https://doi.org/10.1016/j.jcp.2013.07.008.

[18] Markesteijn, A. P., and Karabasov, S. A., "CABARET solutions on graphics processing units for NASA jets: Grid sensitivity and unsteady inflow condition effect," *Comptes Rendus Mécanique*, Vol. 346, No. 10, 2018, pp. 948–963. https://doi.org/https://doi.org/10.1016/j.crme.2018.07.004, URL https://www.sciencedirect.com/science/article/pii/S1631072118301505, jet noise modelling and control / Modélisation et contrôle du bruit de jet.

[19] Semiletov, V., and Karabasov, S., "Cabaret Scheme for Computational Aero Acoustics: Extension to Asynchronous Time Stepping and 3D Flow Modelling," *International Journal of Aeroacoustics*, Vol. 13, No. 3-4, 2014, pp. 321–336. https://doi.org/10.1260/1475-472X.13.3-4.321, URL https://doi.org/10.1260/1475-472X.13.3-4.321.

[20] Faranosov, G., Goloviznin, V., Karabasov, S., Kondakov, V., Kopiev, V., and Zaitsev, M., "CABARET method on unstructured hexahedral grids for jet noise computation," *Computers Fluids*, Vol. 88, 2013, pp. 165–179.

[21] Semiletov, V. A., and Karabasov, S. A., "A volume integral implementation of the Goldstein generalised acoustic analogy for unsteady flow simulations," *Journal of Fluid Mechanics*, Vol. 853, 2018, p. 461–487. https://doi.org/10.1017/jfm.2018.572.

[22] Markesteijn, A. P., and Karabasov, S. A., "Simulations of co-axial jet flows on graphics processing units: the flow and noise analysis," *Philosophical Transactions of the Royal Society A: Mathematical, Physical and Engineering Sciences*, Vol. 377, No. 2159, 2019, p. 20190083. https://doi.org/10.1098/rsta.2019.0083, URL https://royalsocietypublishing.org/doi/abs/10.1098/rsta.2019.0083.

[23] Markesteijn, A. P., Gryazev, V., Karabasov, S. A., Ayupov, R. S., Benderskiy, L. A., and Lyubimov, D. A., "Flow and Noise Predictions of Coaxial Jets," *AIAA Journal*, Vol. 58, No. 12, 2020, pp. 5280–5293.

[24] Abid, H. A., Markesteijn, A. P., and Karabasov, S. A., *Trailing Edge Noise Modelling of Flow over NACA Airfoils Informed by LES*, ???? https://doi.org/10.2514/6.2021-2233, URL https://arc.aiaa.org/doi/abs/10.2514/6.2021-2233.

[25] Abid, H. A., Stalnov, O., and Karabasov, S. A., *Comparative Analysis of Low Order Wall Pressure Spectrum Models for Trailing Edge Noise Based in Amiet Theory*, ???? https://doi.org/10.2514/6.2021-2231, URL https://arc.aiaa.org/doi/abs/10.2514/6.2021-2231.

[26] Kamliya Jawahar, H., Baskaran, K., and Azarpeyvand, M., "Unsteady Characteristics of Mode Oscillation for\Screeching Jets," *AIAA AVIATION 2021 FORUM*, 2021, p. 2279.

[27] Kamliya Jawahar, H., Meloni, S., Camussi, R., and Azarpeyvand, M., "Experimental Investigation on the Jet Noise Sources for Chevron Nozzles in Under-expanded Condition," *AIAA AVIATION 2021 FORUM*, 2021, p. 2181.

[28] Kamliya Jawahar, H., and Azarpeyvand, M., "Trailing-edge Treatments for Jet-installation Noise Reduction," *AIAA AVIATION 2021 FORUM*, 2021, p. 2185.

[29] Kamliya Jawahar, H., and Azarpeyvand, M., "On Investigating the Hydrodynamic Field for Jets with and without Installation Effects," *AIAA AVIATION 2022 FORUM*, 2022.

[30] Park, I. G., "Wall-modeled large-eddy simulation of a separated flow over the NASA wall-mounted hump," *Annual Research Briefs (Center for Turbulence Research)*, , No. 2006, 2015, pp. 145–160.

[31] Mukha, T., Rezaeiravesh, S., and Liefvendahl, M., "A library for wall-modelled large-eddy simulation based on OpenFOAM technology," *Computer Physics Communications*, Vol. 239, 2019, pp. 204–224. https://doi.org/10.1016/j.cpc.2019.01.016.

[32] Ffowcs Williams, J. E., Hawkings, D. L., and Lighthill, M. J., "Sound generation by turbulence and surfaces in arbitrary motion," *Philosophical Transactions of the Royal Society of London. Series A, Mathematical and Physical Sciences*, Vol. 264, No. 1151, 1969, pp. 321–342. https://doi.org/10.1098/rsta.1969.0031.

[33] Lyu, B., and Dowling, A., *Noise Prediction for Installed Jet*, ???? https://doi.org/10.2514/6.2016-2986, URL https://arc.aiaa.org/doi/abs/10.2514/6.2016-2986.